Exploring the Formation of Calcium Orthophosphate-Pyrophosphate Chemical Gardens

Hughes, Erik A. B.; Jones-salkey, Owen; Forey, Prescillia; Chipara, Miruna; Grover, Liam M.

DOI:
10.1002/syst.202000062

Chemistry Europe
European Chemical Societies Publishing

Special Collection

Exploring the Formation of Calcium Orthophosphate-Pyrophosphate Chemical Gardens

Erik A. B. Hughes,*[a, b] Owen Jones-Salkey,[a] Prescillia Forey,[c] Miruna Chipara,[a] and Liam M. Grover*[a]

Chemical gardens are characterised by the self-assembly of mineralised abiotic architectures. Utilising the fundamental building blocks of bone mineral, namely calcium and orthophosphate ions, chemical gardens that recapitulate microstructural and compositional features of hard tissue can be grown. Interplay between orthophosphate and pyrophosphate species is highly relevant to natural mineral deposition processes, though this has yet to be explored in the context of generating biologically relevant chemical gardens. Here, tubular calcium orthophosphate-pyrophosphate chemical gardens were grown from the interface between calcium loaded hydrogels ($[Ca^{2+}] = 1$ M) layered with different orthophosphate-pyrophosphate solutions ($[Pi] + [PPi] = 0.7$ M). We determine the effect of solution pyrophosphate content on chemical garden morphology and growth rate. Extracted structures were analysed by means of powder X-ray diffraction (XRD), Raman spectroscopy, scanning electron microscopy (SEM) and X-ray fluorescence spectroscopy (XRF), revealing orthophosphate-pyrophosphate solution dependent differences in precipitated mineral crystallinity, composition and microstructure, respectively. Lastly, the potential application of the structures is discussed in the context of tissue engineering and regenerative medicine.

1. Introduction

Chemical gardens typically describe the self-assembly of abiotic plant-like precipitates that emerge within minutes following the immersion of metal ion salt seeds in anionic solutions. Despite being completely abiotic, they are often described as growing due to their biologically mimetic appearance. Reactant cation and anionic species can vary greatly, providing a plethora of chemical garden systems. Silicate based chemical gardens are some of the most extensively studied formations, which have been grown from salt seeds of barium, calcium, cobalt, manganese, and nickel, layered with silicate solutions (otherwise known as water glass).[1,2] As well as silicate, anionic reservoirs of carbonate and orthophosphate also provide utilisable media for the formation of life-like self-assemblies from metal ion salts.

In recent decades, the increased interest in chemical garden systems has given rise to a new multidisciplinary field of study, termed "Chemobrionics".[3] Research undertaken in this field has provided a great deal of insight into the mechanisms of chemical garden formation.[4] When a cationic salt seed is dropped into a reservoir of anionic solution, the seed begins to dissolve, leading to the precipitation of a semi-permeable membrane that separates the remaining undissolved seed and the outer solution. Steep gradients in pH and ion concentration provide chemical driving forces that promote the continued dissolution of the seed, which increases internal osmotic pressure. Eventually, the osmotic pressure is relieved by rupturing the semi-permeable membrane, releasing streams of cation rich fluid into the anionic reservoir. The ensuing organisation of precipitate generates life-like morphologies, which continue to grow over repeating cycles of osmotic pressure build up and release until the reactants are depleted or a state of near equilibrium is reached. Common morphologies including tubular, branching and bulbous architectures that arise dependent on reactant selection, concentration and experimental set-up.

In addition to using salt seeds for chemical garden formation, structures can also be grown from pellets of reactant,[5] as well as at hydrogel-solution interfaces,[6] with formation occurring through mechanistically comparable pathways. Additionally, pump-driven systems have been developed that involve the mechanical injection of cationic solutions into pools of anionic reactant. Injection-based approaches provide a means of forming chemical gardens under controllable growth regimes by adjusting experimental parameters, such as flow rate,[7] as well as the exploration of spatially confined systems that have led to the discovery of new morphologies, such as spirals, flowers and worms.[8]

The chemical and physical driving forces behind chemical gardens are now known to be responsible for the formation of geological phenomena, including the formation of chimney

[a] Dr. E. A. B. Hughes, O. Jones-Salkey, M. Chipara, Prof. L. M. Grover
School of Chemical Engineering
University of Birmingham, Birmingham
B15 2TT (UK)
E-mail: e.a.b.hughes@bham.ac.uk
l.m.grover@bham.ac.uk
[b] Dr. E. A. B. Hughes
NIHR Surgical Reconstruction and Microbiology Research Centre
Queen Elizabeth Hospital
Birmingham (UK)
[c] P. Forey
Ensaia, Université De Lorraine
34 Cours Léopold, CS 25233, F-54052, Nancy (France)

Special Collection An invited contribution to a Special Collection on Chemobrionics

structures at the sites of deep sea hydrothermal vents,[9,10] linking chemical gardens to the origins of life. On prebiotic earth, these formations may have facilitated the harvesting of energy across chemical gradients,[11] possibly promoting the very first reactions to yield molecules essential to life, such as amino acids[12] and RNA oligomers.[13] Moreover, chemical gardens are also being utilised as a source of inspiration for the development of novel technologies and systems, including biomedical materials,[14,15] chemical motors[16] and chemical clocks.[17]

In our previous work, we reported the formation of chemical gardens from calcium (Ca^{2+}) and orthophosphate (Pi, HPO_4^{2-} and PO_4^{3-}) reactants.[14,18] Utilisation of the fundamental building blocks of bone mineral promoted the self-assembly of tubular structures comprised predominantly of an apatitic bone like phase (i.e. $Ca_{10}(PO_4)_6(OH)_2$). As well as orthophosphate, condensed phosphates such as inorganic pyrophosphate (PPi, $P_2O_7^{4-}$), also play a key role in human biomineralisation processes.[19] Pyrophosphate is a potent mineralisation regulator that is capable of hindering the nucleation and subsequent crystal growth of apatatic mineral.[20–22] In this context, the formation of calcium orthophosphate-pyrophosphate chemical gardens presents an interesting prospect. In particular, the interplay of orthophosphate and pyrophosphate is highly relevant when considering natural mineral deposition processes.

In this paper, we extend our exploration of calcium orthophosphate chemical garden systems to those composed of calcium, orthophosphate and pyrophosphate species. Our results demonstrate that altering the orthophosphate-pyrophosphate concentration ratio incurs unique differences in overall structural morphology, growth rate, composition and microstructure. Moreover, subtle adjustments in pH can alter the growth rate of calcium orthophosphate-pyrophosphate chemical gardens by influencing the inhibitory properties of pyrophosphate during the self-assembly of tubular apatitic structures. Finally, we also highlight the relevance of these chemical garden systems to the development of novel materials for biotechnological applications, in particular the potential formulation of biologically responsive biomaterials for the regeneration of hard tissues.

Experimental Section

Growth of Chemical Gardens

Reagents were acquired from Sigma-Aldrich (Gillingham, UK). Calcium nitrate tetrahydrate ($Ca(NO_3)_2{\cdot}4H_2O$, 99%, ACS reagent) was dissolved in deionised water ($[Ca^{2+}] = 1$ M). Agar ($(C_{12}H_{18}O_9)_n$, for microbiology) was added to the solution at 5 wt% and the mixture heated to 80–90°C whilst stirring at 250 rpm. Gel mixture was then decanted into clear 50 ml containers and allowed to cool to room temperature. Set gels were stored in a refrigerated unit at 4 °C overnight. Prior to use, gels were placed in a 60 °C oven for 15 min to remove any condensation.

Dibasic sodium orthophosphate (Na_2HPO_4, ≥ 99.0%, ReagentPlus®) was dissolved in deionised water ($[Pi] = 0.7$ M). Additional solutions ($[Pi + PPi] = 0.7$ M) were also prepared by substituting dibasic sodium orthophosphate for sodium pyrophosphate decahydrate ($Na_4P_2O_7{\cdot}10H_2O$, ≥ 99%, ACS reagent) (Table 1). Solution pH was measured using a calibrated Mettler Toledo™ FiveEasy™ F20 pH/mV Meter (Mettler Toledo, USA). Solutions were layered upon the gel in order to initiate the formation of chemobrionic structures. Tube height was measured every 5 min using a digital set of Vernier callipers. Measurements were taken between the gel/solution interface and the representative height of tubules. After 1 h of growth, a cell strainer sieve was used to collect intact structures, which were gently washed using deionised water. Structures were carefully transferred to glass slides and dried overnight at 60 °C.

Material Characterisation

In order to acquire compositional datasets representative of the average bulk composition of structures, samples were crushed into fine powders prior to X-ray diffraction (XRD) and Raman analysis. For XRD, diffraction patterns were acquired between $2\theta = 5°$–$60°$ with a step of $2\theta = 0.02°$ and step time of 0.5 s/° using a Powder Diffractometer D8 autosampler instrument (Bruker, USA) with the Cu Kα beam line. Matching patterns for known crystalline phases were identified from the International Centre for Diffraction Data (ICDD) database. For Raman spectroscopy, spectra were acquired between Raman shift values of 300–1100 cm^{-1} using an inVia™ Raman microscope (Renishaw Plc, UK) equipped with a monochromatic 532 nm laser and 2400 l/mm grating. Each spectrum consists of three accumulations ($n = 3$). For scanning electron microscopy (SEM), intact samples were adhered onto double adhesive carbon discs attached to aluminium stubs and gold sputter coated. Secondary electron micrographs were collected using a TM 3030 Plus electron microscope (Hitachi, Japan) with the beam power at 10 kV. For X-ray fluorescence (XRF) elemental mapping, intact samples were transferred to a glass slide and analysed using a M4 Tornado instrument (Bruker, USA). Elemental maps were acquired under vacuum (30 mbar) with the X-ray tube operating at a voltage of 50 kV and an anode current of 300 mA. The samples were imaged over a selected area of interest at a scan time of 20 ms/pixel. Each image consists of two accumulations ($n = 2$).

2. Results and Discussion

2.1. Observations of Tubular Growth and Morphology

The primary variable in these experiments was the concentration ratio of orthophosphate to pyrophosphate totalling 0.7 M in the solution phase (Table 1). Figure 1 shows a macroscopic view of tube formation generated by the orthophosphate-pyrophosphate solutions ($[Pi] + [PPi] = 0.7$ M) being

Table 1. Composition of the reactant orthophosphate-pyrophosphate solutions. ($[Pi] + [PPi] = 0.7$ M).

[Pi] [M]	[PPi] [M]	[PPi] [%]
0.7	0	0
0.679	0.021	3
0.658	0.042	6
0.637	0.063	9
0.616	0.084	12
0.595	0.105	15
0.574	0.126	18
0.553	0.147	21

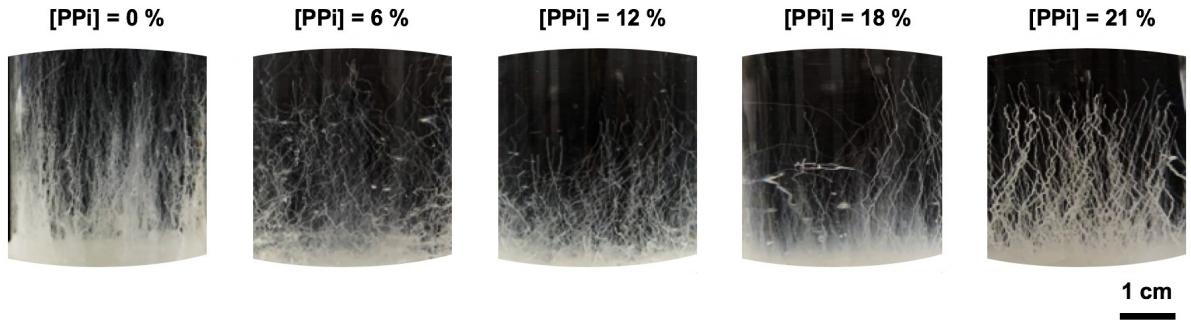

Figure 1. Morphologies of calcium orthophosphate-pyrophosphate chemical gardens grown from calcium loaded hydrogels ($[Ca^{2+}] = 1$ M) and orthophosphate-pyrophosphate solutions ([Pi] + [PPi] = 0.7 M). These images show structures grown for 1 h.

placed onto the hydrogel surface containing calcium ions ($[Ca^{2+}] = 1$ M) after 1 h. Structures form via the same mechanism as a chemical garden developing from a salt seed, with the hydrogel-solution interface facilitating the necessary chemical gradients (osmotic, pH, concentration) to initiate growth.[18] Firstly, an initial semi-permeable calcium orthophosphate-pyrophosphate membrane formed on the surface of the hydrogels, which promotes the advective transport of ions and water from the solution toward the hydrogel phase. This causes a build-up of osmotic pressure at the hydrogel-solution interface. The pressure is subsequently released through streams of calcium ions, which pierce the semipermeable membrane. Upon entering the orthophosphate-pyrophosphate solution reservoirs, precipitation nucleates around the calcium streams, leading to development of tubular architectures. Tubular elongation is maintained through continuing cycles of osmotic pressure that drive the release of calcium ions through the established structures, which contribute to furthered precipitation at the tip of the tube.

Whilst pyrophosphate is an inhibitor of apatite precipitation and crystallisation,[20–22] its presence in these systems did not prevent the formation of chemical garden structures, rather the inclusion of pyrophosphate visibly altered tube population and morphology. In the absence of pyrophosphate, a dense populous of intricate tubular structures was generated, consistent with the formation of purely calcium orthophosphate chemical garden systems for the reactant concentrations employed.[14] As the pyrophosphate content was increased between [PPi] = 6–12%, the chemical gardens appear increasingly sparse and exhibit deviations in upward growth direction, in some respects appearing to bend downwards. Pyrophosphate therefore initially appears to have a detrimental effect on tube development and population, which we observe to be most evident for conditions of [PPi] = 12%. However, as the PPi content is increased beyond 12% in conditions of [PPi] = 18–21%, tube development visibly improved. Therefore, the relationship between tube formation and increasing pyrophosphate concentration was not found to be monotonic within these systems. In terms of appearance, tubes grown from [PPi] = 21% solutions appeared to be of comparable robustness to those formed from [PPi] = 0% solutions. However, the [PPi] = 21% structures were of a more delicate assembly, being the most challenging tubes to retrieve intact from reactant solution.

2.2. Effect of Pyrophosphate Content on Tube Growth Rate

In this particular set of experiments, the pH of the solutions used to initiate growth was not adjusted. Table 2 provides the native pH values of the respective orthophosphate-pyrophosphate solutions. Solution pH was found to increase with the addition of pyrophosphate. Indeed, the low pKa values associated with the PPi ion in alkaline environments means that it readily dissociates, accounting for incremental increases in pH with pyrophosphate addition and subsequent displacement in the solutions.

As shown in Figure 2a, tube height in the *Z* direction was monitored at 5 min intervals over a period of 1 h. Measurements of tube height were taken between the gel/solution interface and the representative height of the majority of tube structures. Measurable changes in growth rate (mm/min) can be determined from the slope of tube height (mm) over time (min). In all cases, there was a linear increase in tube height with time over the first 15 min of formation. The respective initial growth rates are provided in Table 3. Tubes prepared from [PPi] = 0% displayed an approximate growth rate of 1 mm/min, whilst growth rates of tubes grown from solutions containing pyrophosphate were in the range of 1.1–1.5 mm/min. Interestingly, growth rates associated with tubes generated from pyrophosphate containing solutions were observed to reduce at around 20 min to $\leq$ 1 mm/min, whilst tubes grown in the absence of pyrophosphate grew at a consistent rate of 1 mm/min until reaching the growth vessel ceiling at approx-

Table 2. Native pH values for the reactant orthophosphate-pyrophosphate solutions ([Pi] + [PPi] = 0.7 M).

[PPi] [%]	pH value
0	9.35
6	9.45
12	9.54
18	9.6
21	9.64

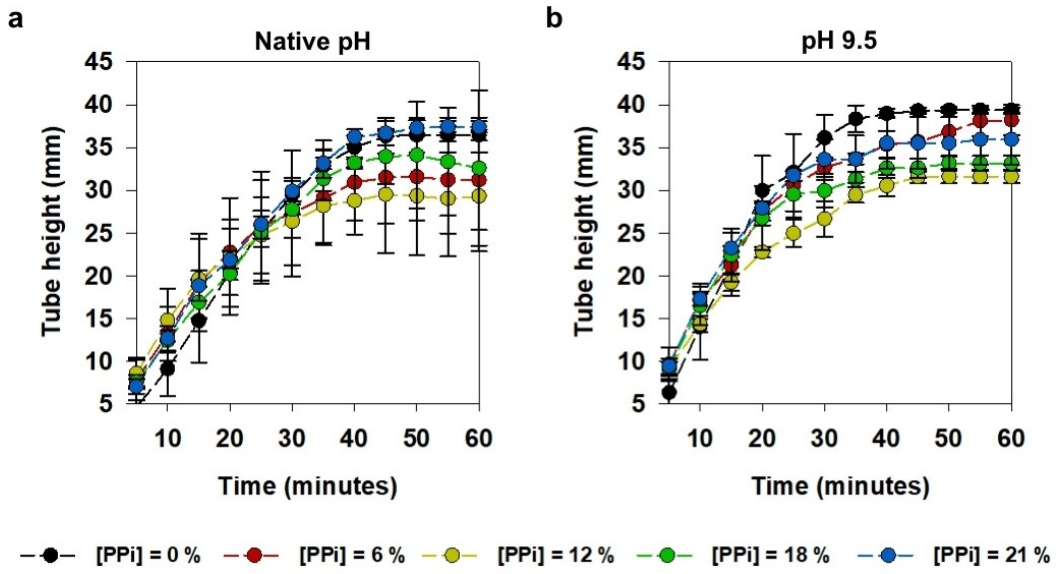

Figure 2. Tube height as a function of time for calcium orthophosphate-pyrophosphate chemical gardens grown from calcium loaded hydrogels ($[Ca^{2+}] = 1$ M) and orthophosphate-pyrophosphate solutions ($[Pi] + [PPi] = 0.7$ M) (a) at native pH (n = 4) and (b) with solutions adjusted to pH 9.5 (n = 4).

Table 3. Initial growth rate of calcium orthophosphate-pyrophosphate chemical gardens grown from calcium loaded hydrogels ($[Ca^{2+}] = 1$ M) and orthophosphate-pyrophosphate solutions ($[Pi] + [PPi] = 0.7$ M) at native pH.

[PPi] [%]	Growth rate [mm/min]
0	0.97
6	1.26
12	1.44
18	1.11
21	1.24

Table 4. Initial growth rate of calcium orthophosphate-pyrophosphate chemical gardens grown from calcium loaded hydrogels ($[Ca^{2+}] = 1$ M) and orthophosphate-pyrophosphate solutions ($[Pi] + [PPi] = 0.7$ M) adjusted to pH 9.5.

[PPi] [%]	Growth rate [mm/min]
0	1.34
6	1.40
12	1.28
18	1.49
21	1.55

imately 35 min. Growth velocities in all cases levelled off by 40 min (approximately 0 mm/min). This resulted in notable differences in the final tube height as a consequence of pyrophosphate content, with [PPi] = 12% being most detrimental to tube development overall, despite these structures being associated with the greatest initial growth rate of 1.44 mm/min. Tubes grown from [PPi] = 0% and [PPi] = 21% demonstrated comparable final growth heights.

2.3. Effect of pH on Tube Growth Rate

Within chemobrionic systems, pH gradients between cationic and anionic species can contribute a major chemical driving force capable of influencing formation and structure. Therefore, growth experiments were also performed with all solutions adjusted to pH 9.5 in order to understand the influence of pH on tube formation rate.

As shown in Figure 2b, tube height in the *Z* direction was monitored at 5 min intervals over a period of 1 h for pH adjusted solutions. The respective initial growth rates are provided in Table 4. Adjusting the pH of [PPi] = 0% solution from 9.35 to 9.5 increased the growth rate from approximately 1 mm/min to 1.34 mm/min, which was comparable to the initial growth velocities displayed by tubes grown from solutions containing pyrophosphate prior to pH adjustment. As the hydrogel phase is slightly acidic, increasing the alkalinity of the [PPi] = 0–6% solutions effectively steepens the pH gradient between hydrogel and solution phases. This may promote the elevated advective transport of ions at the hydrogel-solution interface, which in turn augments the tubular growth rate. Interestingly, the growth rate of tubes grown from [PPi] = 18–21% solutions also increased, despite the pH of the solutions being reduced relative to native pH of these solutions. Additionally, the apparent growth ceiling of tubes grown from [PPi] = 18–21% solutions was notably reduced by adjustment of the pH to 9.5. Compared to tubes grown from [PPi] = 0% solutions adjusted to pH 9.5, adjusting the pH of [PPi] = 21% solutions from 9.64 to 9.5 resulted in a 5 mm deficit in final tube height between these tubes. Although [PPi] = 12% solutions required the smallest adjustment in pH from 9.54 to 9.5, this condition remained the most detrimental to tube development,

In order to explore the effects of pH alteration and PPi content further, tubes were grown from [PPi] = 0% and [PPi] = 12% solutions adjusted to pH 9. Tube growth was compared to structures grown from solutions adjusted to pH 9.5. As shown

in Figure 3a, the initial growth rate of tubes prepared with [PPi] = 0% solutions exceeded those of tubes prepared from [PPi] = 12% solutions by approximately 0.5 mm/min when the solutions were adjusted to pH 9. Comparably, Figure 3b reveals that when the solutions were adjusted to pH 9.5, the distinction between initial growth rates was less extensive, differing by 0.1 mm/min. Whilst tubes form more rapidly in the absence of pyrophosphate, the differences in growth are more apparent when the pH was decreased. There were also apparent differences in the final growth height, with tubes grown with [PPi] = 12% solutions adjusted to pH 9 failing to grow beyond 25 mm, whereas adjustment of solutions to pH 9.5 resulted in tubes reaching up to 30 mm. The deficit in final tube heights was therefore approximately 15 mm and 10 mm, respectively, between these tubes and those grown from [PPi] = 0% solutions. Finally, [PPi] = 12% solutions generally resulted in fewer tubes compared to [PPi] = 0% solutions, however, the population of forming tubes was further diminished by adjustment of [PPi] = 12% solutions to pH 9.

Regarding calcium orthophosphate-pyrophosphate chemical garden systems, the results imply that adjustments in solution pH influence both the chemical driving forces that determine initial growth rate, as well as the apparent growth ceiling. Given that pyrophosphate inhibitor activity is enhanced at lower pH values,[21] the nucleation of structurally supportive apatitic mineral may be impeded when the pH is adjusted toward pH 9, possibly accounting for deviations in upward growth direction and the formation of fewer tubes overall.

2.4. Tube Composition

X-ray diffraction (XRD) patterns are shown in Figure 4a. For tubes grown from 0% = [PPi] solutions, the diffraction pattern is consistent with that of apatitic calcium orthophosphate and

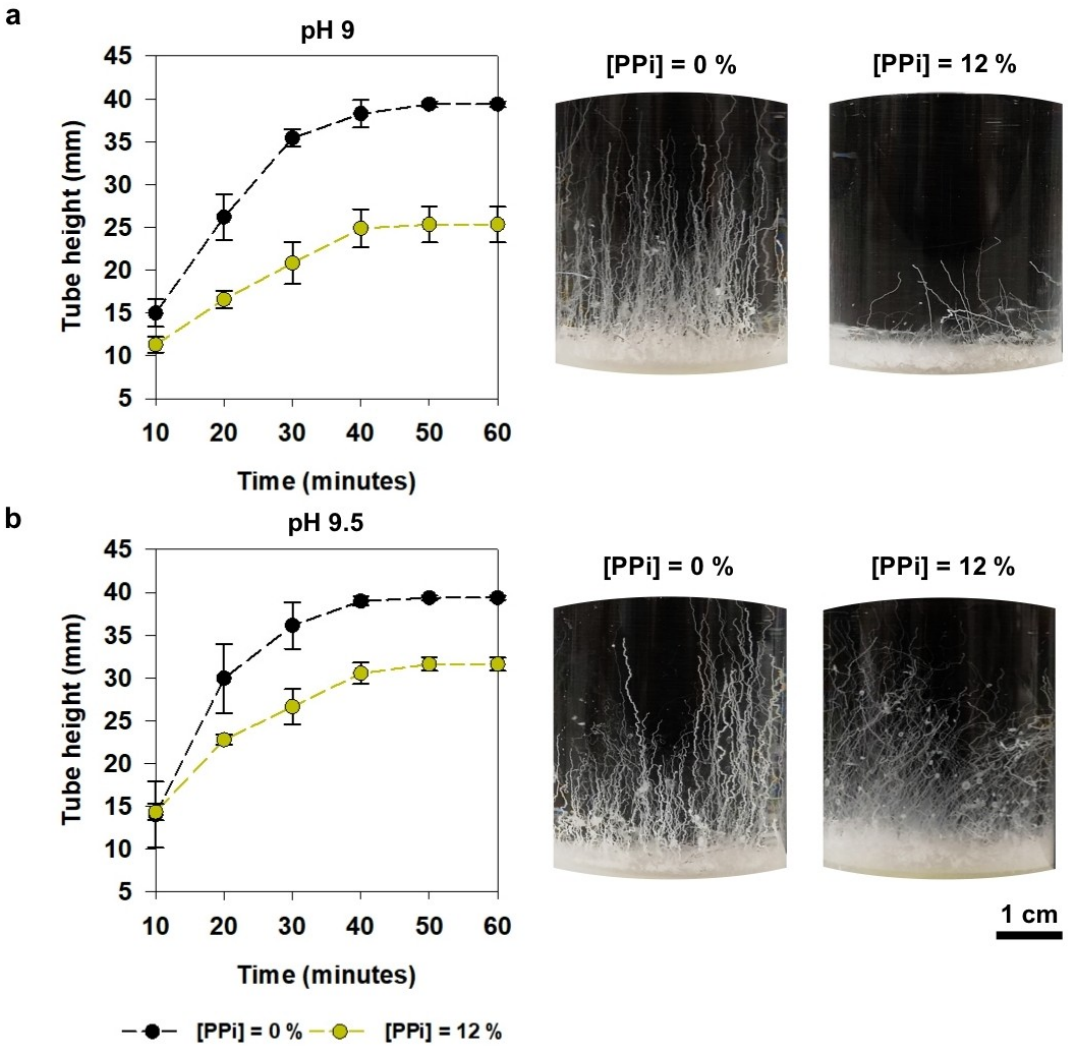

Figure 3. Tube height as a function of time for calcium orthophosphate-pyrophosphate chemical gardens grown from calcium loaded hydrogel ($[Ca^{2+}] = 1$ M) and [PPi] = 12% solutions (a) adjusted to pH 9 (n = 4) and (b) adjusted to pH 9.5 (n = 4). Tube morphologies for the respective conditions are also shown. These images show structures grown for 1 h.

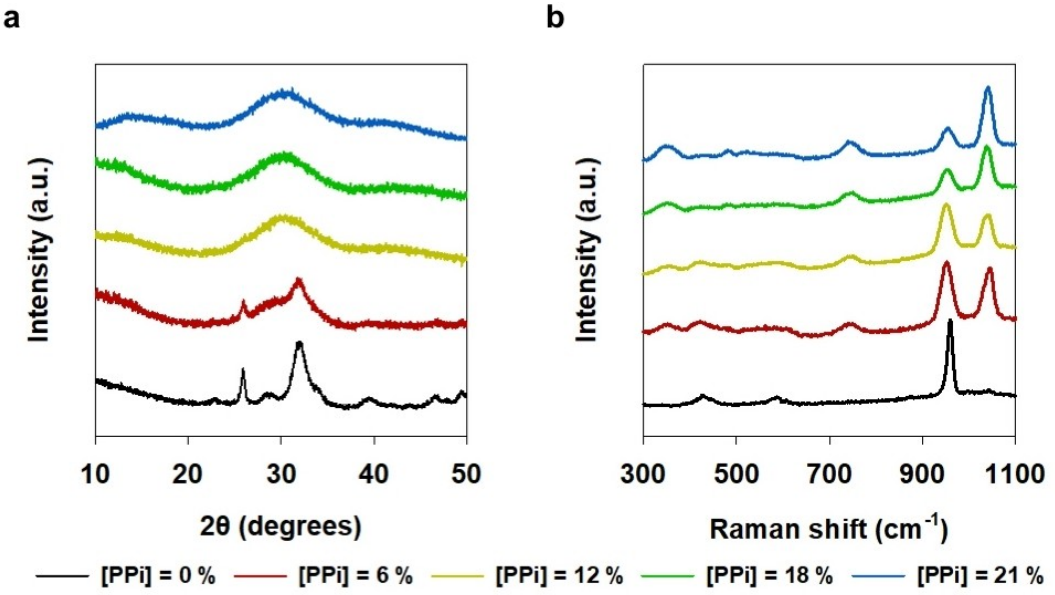

Figure 4. (a) Powder X-ray diffraction patterns and (b) Raman spectra for calcium orthophosphate-pyrophosphate chemical gardens grown from calcium loaded hydrogels ($[Ca^{2+}] = 1$ M) and orthophosphate-pyrophosphate solutions ($[Pi] + [PPi] = 0.7$ M).

was matched to ICDD pattern 01-074-9761 for hydroxyapatite. For tubes grown from [PPi] = 6% solutions, the corresponding hydroxyapatite peaks appear less defined whilst the background intensity increases. For tubes grown from [PPi] = 12–21% solutions, the patterns consist broad signal between 26–32° 2θ degrees, indicating that the mineral precipitated is X-ray amorphous. It has been determined that pyrophosphate inhibits crystallisation by adsorbing onto sites of hydroxyapatite crystal growth, which prevents further binding of ionic building blocks (i.e. calcium and orthophosphate).[20] In effect, this mechanism increases the temporal stability of amorphous calcium orthophosphate,[22] accounting for the poorer crystallinity attributed to precipitates grown from solutions of increasing pyrophosphate content.

Raman spectra are shown in Figure 4b. The Raman spectrum of tubes grown from [PPi] = 0% solutions shows an intense peak located at 960 cm^{-1}, which correlates specifically to the symmetric stretching vibration mode of the PO_4 group as found in hydroxyapatite.[23] Additional peaks located at 430 cm^{-1}, 590 cm^{-1} and 1045 cm^{-1} are consistent with hydroxyapatite PO_4 group symmetric bending, asymmetric bending and asymmetric stretching, respectively. For tubes grown from [PPi] = 6–21% solutions, the apatite symmetric stretching peak becomes broader and is downshifted to approximately 950–590 cm^{-1}, indicative of an amorphous apatitic phase.[24] Further, peaks indicative of apatite symmetric bending, asymmetric bending and asymmetric stretching are substantially diminished. Peaks associated with PPi content appear at approximately 740 cm^{-1} and 1040 cm^{-1}, indicative of P–O–P and P–O stretching vibrations respectively.[25] As the pyrophosphate content increases, the intensity of the 1040 cm^{-1} peak is enhanced whilst the corresponding intensity of the apatite symmetric stretching peak between 950–590 cm^{-1} decreases.

Calcium orthophosphate-pyrophosphate structures therefore appear to be comprised of amorphous phases of both apatite and calcium pyrophosphate mineral. Quantitative peak intensity variations associated with the respective phases suggests that the overall composition of these chemical gardens can be systematically manipulated by orthophosphate-pyrophosphate solution selection.

2.5. Tube Microstructure

Microstructural features and surface topology of precipitated structures was analysed using scanning electron microscopy (SEM) as shown in Figure 5. The typical radius of the tubes analysed ranged between 50–100 μm. Tube wall thickness was also observed to range between 5–10 μm. Both the outside and inside facing walls of tubes grown from [PPi] = 0% solutions showed a porous structuring, made up of closely packed micron sized spheres, consistent with the appearance of apatite precipitated in previous systems.[14,18] The outside and inside surfaces are separated by a distinct 2–5 μm thick interface with denser structuring. This intermediate tube wall layer may act as a substrate that supports the development and evolution the resulting microstructure observed.

Micrographs reveal changes in microstructure as the pyrophosphate content of the reactant solution is incrementally increased. Tubes grown from [PPi] = 6–18% solutions also exhibit spherical microstructuring, similar to those grown from [PPi] = 0% solutions, however, there are distinct regions of a secondary amorphous microstructure that appears to coat tube surfaces, possibly resulting from the addition precipitation of an amorphous calcium pyrophosphate phase. For some of the tubes grown from [PPi] = 6% solutions, we observed delamina-

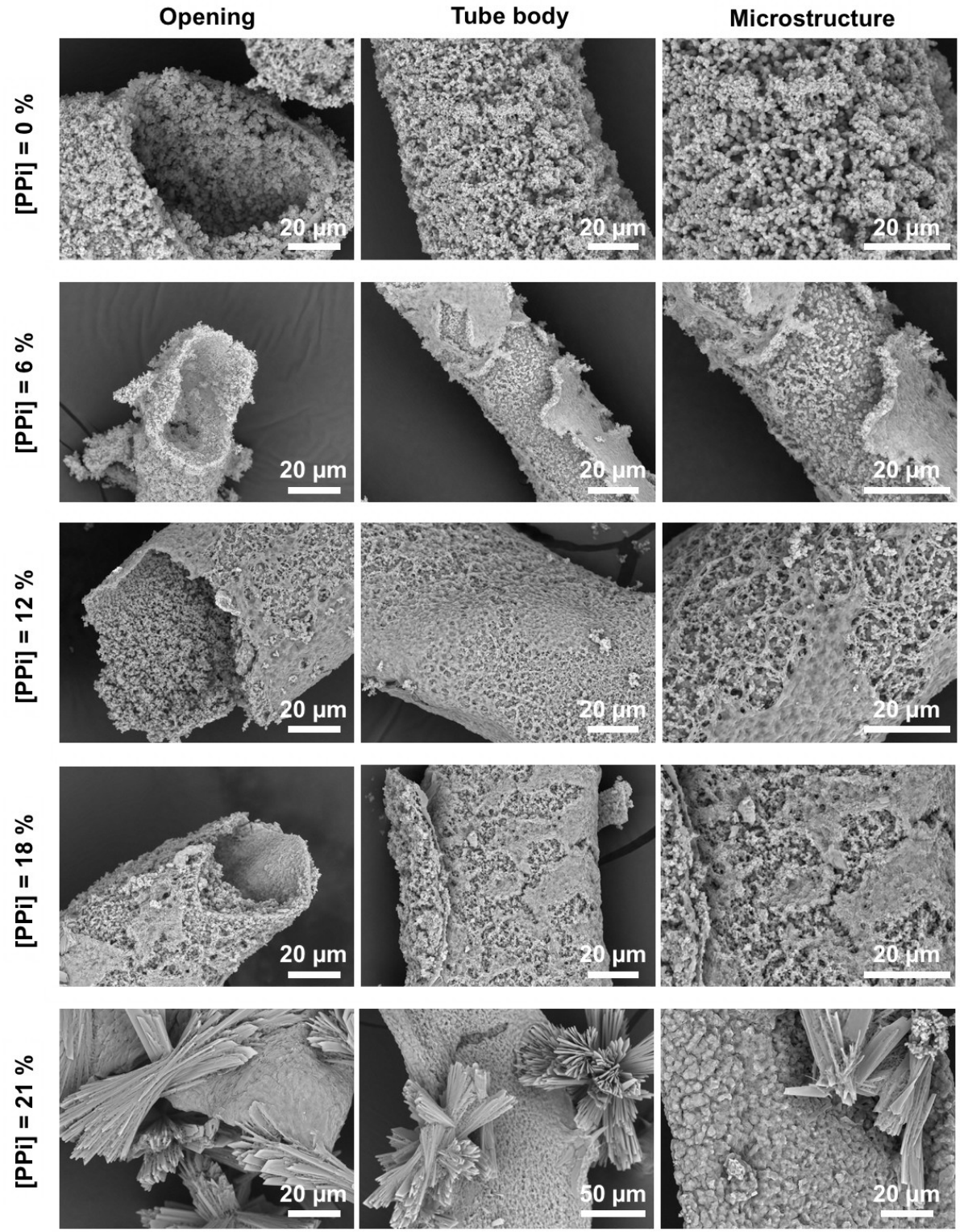

Figure 5. Scanning electron microscopy (SEM) images of calcium orthophosphate-pyrophosphate chemical gardens grown from calcium loaded hydrogels ($[Ca^{2+}] = 1$ M) and orthophosphate-pyrophosphate solutions ([Pi] + [PPi] = 0.7 M).

tion of this secondary microstructure, revealing the thickness of the coating to be in the range of 3–5 µm. For tubes grown from [PPi] = 12–18%, the secondary microstructure appears to form a thin film over the underlying primary spherical microstructure, perhaps no more than 1–2 µm in thickness. Further compositional analysis of the surfaces of tubes grown from [PPi] = 0%

solutions and [PPi] = 12% solutions was investigated with X-ray fluorescence (XRF) spectroscopy. As shown in Figure 6, elemental maps revealed distinct phosphorous rich regions upon the outer walls of tubes grown from [PPi] = 12%. This suggests that pyrophosphate species are a prevalent constitutional component of the secondary microstructure, whilst the underlying microstructure is compositionally comparable to that of the surface of tubes prepared with [PPi] = 0% solutions.

Tubes grown from [PPi] = 21% show a dramatic shift in microstructural features. Tube walls consisted of a closely packed arrangement of individual particulates that were approximately 3–5 μm in size. This well aggregated microstructure may contribute to the structural stability of these formations, accounting for little deviation in upward growth. In addition, their amorphous nature explains their fragility, making them difficult to retrieve intact as mentioned prior. High aspect ratio blade morphologies were also observed, suggesting crystal formation at the tube surface. Discrete star-burst arrangements are consistent with the structuring of calcium pyrophosphate, specifically crystals with the chemical formula $Ca_2P_2O_7.4H_2O$.[25] In some micrographs, these crystal formations appear to have formed independently of tube structures, suggesting they may be formed as a consequence of the washing and drying procedures applied (i.e. dissolution followed by reprecipitation). Alternatively, the crystals may have become detached following formation at the tube surface.

2.6. Potential Application of Calcium Orthophosphate-Pyrophosphate Chemical Gardens

Whilst this paper primarily focuses on characterising the growth, structure and composition of calcium orthophosphate-pyrophosphate chemical gardens, it is important to consider the potential applications of such materials. Some proposed technological applications of materials derived from chemobrionic principles include biomaterials, catalysts, microfluidic networks and gas exchange substrates.[3] We have previously shown that utilising the fundamental ionic building blocks of bone mineral, namely calcium and orthophosphate, biologically analogous structures can be derived.[18] Further, given that such frameworks facilitate the favourable attachment and prosperity of various cell types, including bone derived mesenchymal stem cells,[14,26] there is evident scope to further explore these materials in the context of tissue engineering and regenerative medicine applications.

In terms of composition, calcium orthophosphate based biomaterials have been extensively investigated as potential bone substitutes.[27–29] Hydroxyapatite ($Ca_{10}(PO_4)_6(OH)_2$) or calcium deficient hydroxyapatite ($Ca_9(PO_4)_5HPO_4OH$), brushite ($CaHPO_4.2H_2O$) and β-tricalcium orthophosphate (β-$Ca_3(PO_4)_2$) are commonly used substitute biomaterials due to their chemical similarity to that of the bone mineral.[30] Interestingly, calcium pyrophosphate phases have been shown to enhance hard tissue regeneration by eliciting fundamental mechanisms found within biomineralisation pathways.[31] Pyrophosphate occurs naturally in the human body and is involved in more than 170 biological reactions.[32] Within bone and other tissues,

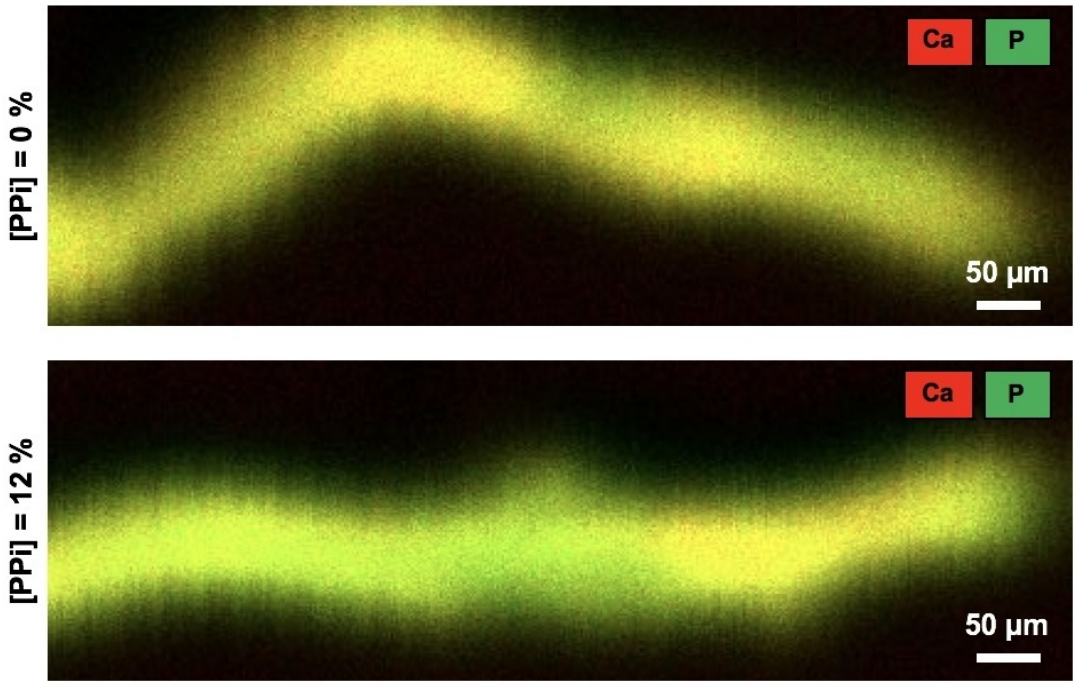

Figure 6. X-ray fluorescence (XRF) elemental maps of calcium orthophosphate-pyrophosphate chemical gardens grown from calcium loaded hydrogel ($[Ca^{2+}] = 1$ M) and [PPi] = 0% or [PPi] = 12% solutions.

pyrophosphate promotes the activity of alkaline phosphatase (ALP),[33] an enzyme that hydrolytically cleaves extracellular pyrophosphate to produce orthophosphate ions [Equation (1)]. This effectively reduces a proportion of mineral inhibiting pyrophosphate species whilst simultaneously supplying orthophosphate that can be utilised for the deposition of new bone mineral.

$$P_2O_7^{4-} + H_2O \rightarrow 2PO_4^{3-} + 2H^+ \quad (1)$$

Materials structured across the nano- and microscale have also gained particular interest for hard tissue regeneration, with desirable properties including high surface area, hierarchal porosity, enhanced loading/release behaviour and ability to influence cellular interactions.[34] For instance, the regenerative potential of microflowers composed of calcium orthophosphate and calcium pyrophosphate phases has been investigated both *in vitro* and *in vivo*.[35] Interestingly, the composition and structuring of these materials stimulated the osteogenic differentiation of mesenchymal stem cells and promoted bone formation that resembled natural tissue within rat calvarial critical size defects. Tubular calcium orthophosphate-pyrophosphate chemical gardens may therefore present another biologically responsive group of structured materials of interest for future study of regenerative capabilities.

The ability of chemical gardens to encapsulate and release therapeutic cargos only adds to the potential usability of these materials in the field of regenerative medicine and tissue engineering.[36–38] Incorporating growth factors and proteins such as vascular endothelial growth factor (VEGF),[39–41] bone morphogenic protein-2 (BMP-2),[41,42] and bone morphogenic protein-7 (BMP-7), also known as recombinant human osteogenic protein-1 (OP-1),[43] could improve the bone regeneration process further. Alternatively, the encapsulation of iron oxide ions within a calcium pyrophosphate phase has also been demonstrated to promote osteoblast growth and osteogenesis.[44]

3. Conclusions

In this paper, the formation of novel calcium orthophosphate-pyrophosphate chemical garden systems was explored for the first time. Tubular structures were grown from calcium loaded hydrogels ($[Ca^{2+}] = 1$ M) layered orthophosphate-pyrophosphate solutions ($[Pi] + [PPi] = 0.7$ M). The complex interplay of orthophosphate and pyrophosphate species was highlighted by the measurable alterations in morphology and growth rate dependent on solution pyrophosphate content, with solutions of [PPi] = 12% being the most detrimental to structural development. For orthophosphate-pyrophosphate solutions with a native pH below 9.5, increasing the alkalinity accelerated the growth of chemical gardens. This was postulated to occur through (i) the steepening of the pH gradient between the hydrogel-solution, promoting enhanced advective transport of ionic reactant contributing to structural formation, and (ii) the mineral inhibiting properties of pyrophosphate are diminished at higher pH values, positively impacting the nucleation of structurally supportive apatitic mineral, leading to fewer deviations in upward growth.

Compositional analysis using XRD and Raman spectroscopy revealed the calcium orthophosphate-pyrophosphate chemical gardens to comprise of highly amorphous apatitic calcium orthophosphate and calcium pyrophosphate phases. Micrographs acquired by SEM and XRF elemental mapping confirmed the development new microstructural features following incremental increases in solution pyrophosphate content, including distinct surface layers and crystal formations.

As well as to gain new knowledge of physically and chemically driven complex systems, the continued research of chemical gardens is opening exciting new avenues of exploration for applied science and engineering. Based on their biologically relevant composition, calcium orthophosphate-pyrophosphate chemical gardens may be of interest as novel materials for biotechnological application. Thus, our study provides further scope for the exploration of these chemical gardens systems as prospective components of tissue engineering scaffolds and biologically responsive biomaterials.

Acknowledgments

This study was funded by the National Institute for Health Research (NIHR) Surgical Reconstruction and Microbiology Research Centre (SRMRC). The views expressed are those of the authors and not necessarily those of the NIHR or the Department of Health and Social Care. Additionally, the authors acknowledge the Chemobrionics COST Action (CA17120).

Conflict of Interest

The authors declare no conflict of interest.

Keywords: calcium phosphates · chemical gardens · chemobrionics · self-assembly · tubular microstructures

[1] J. H. E. Cartwright, B. Escribano, C. I. Sainz-Díaz, *Langmuir.* **2011**, *27*, 3286–3293.
[2] J. H. E. Cartwright, B. Escribano, S. Khokhlov, C. I. Sainz-Díaz, *Phys. Chem. Chem. Phys.* **2011**, *13*, 1030–1036.
[3] L. M. Barge, S. S. S. Cardoso, J. H. E. Cartwright, G. J. T. Cooper, L. Cronin, A. De Wit, I. J. Doloboff, B. Escribano, R. E. Goldstein, F. Haudin, *et al., Chem. Rev.* **2015**, *115*, 8652–8703.
[4] J. H. E. Cartwright, J. M. García-Ruiz, M. L. Novella, F. Otálora, *J. Colloid Interface Sci.* **2002**, *256*, 351–359.
[5] P. J. Fryfogle, E. J. Nelson, J. J. Pagano, *Colloids Surf. A* **2015**, *485*, 84–90.
[6] C. J. Steenbjerg Ibsen, B. F. Mikladal, U. Bjørnholt Jensen, H. Birkedal, *Chem. A Eur. J.* **2014**, *20*, 16112–16120.
[7] B. C. Batista, O. Steinbock, *Chem. Commun.* **2015**, *51*, 12962–12965.
[8] F. Haudin, V. Brasiliense, J. H. E. Cartwright, F. Brau, A. De Wit, *Phys. Chem. Chem. Phys.* **2015**, *17*, 12804–12811.
[9] S. S. S. Cardoso, J. H. E. Cartwright, *Proc. R. Soc. A Math. Phys. Eng. Sci.* **2017**, *473*, 20170387.
[10] L. M. Barge, Y. Abedian, I. J. Doloboff, J. E. Nuñez, M. J. Russell, R. D. Kidd, I. Kanik, *JoVE.* **2015**, *18*, e53015.

[11] L. M. Barge, Y. Abedian, M. J. Russell, I. J. Doloboff, J. H. E. Cartwright, R. D. Kidd, I. Kanik, *Angew. Chem. Int. Ed.* **2015**, *54*, 8184–8187; *Angew. Chem.* **2015**, *127*, 8302–8305.
[12] L. M. Barge, E. Flores, M. M. Baum, D. G. VanderVelde, M. J. Russell, *Proc. Natl. Acad. Sci. USA* **2019**, *116*, 4828–4833.
[13] B. T. Burcar, L. M. Barge, D. Trail, E. B. Watson, M. J. Russell, L. B. McGown, *Astrobiology.* **2015**, *15*, 509–522.
[14] E. A. B. Hughes, M. Chipara, T. Hall, R. L. Williams, L. M. Grover, *Biomater. Sci.* **2020**, *8*, 812–822.
[15] E. A. B. Hughes, S. C. Cox, M. E. Cooke, O. G. Davies, R. L. Williams, T. J. Hall, L. M. Grover, *Adv. Healthcare Mater.* **2018**, *7*, 1701166.
[16] M. Frenkel, V. Multanen, R. Grynyov, A. Musin, Y. Bormashenko, E. Bormashenko, *Sci. Rep.* **2017**, *7*, 3930.
[17] Y. Ding, C. M. Gutiérrez-Ariza, C. Ignacio Sainz-Díaz, J. H. E. Cartwright, S. S. S. Cardoso, *Angew. Chem. Int. Ed.* **2019**, *58*, 6207–6213.
[18] E. A. B. Hughes, R. L. Williams, S. C. Cox, L. M. Grover, *Langmuir.* **2017**, *33*, 2059–2067.
[19] E. A. B. Hughes, T. E. Robinson, D. B. Bassett, S. C. Cox, L. M. Grover, *J. Mater. Chem. B.* **2019**, *7*, 7460–7470.
[20] W. N. Addison, F. Azari, E. S. Sørensen, M. T. Kaartinen, M. D. McKee, *J. Biol. Chem.* **2007**, *282*, 15872–15883.
[21] J. W. L. Wilson, P. G. Werness, L. H. Smith, *J. Urol.* **1985**, *134*, 1255–1258.
[22] C. J. Ibsen Steenberg, H. Birkedal, *Minerals.* **2018**, *8*, 65.
[23] S. Koutsopoulos, *J. Biomed. Mater. Res.* **2002**, *62*, 600–612.
[24] J. A. Stammeier, B. Purgstaller, D. Hippler, V. Mavromatis, M. Dietzel, *MethodsX.* **2018**, *5*, 1241–1250.
[25] P. Gras, C. Rey, O. Marsan, S. Sarda, C. Combes, *Eur. J. Inorg. Chem.* **2013**, *34*, 5886–5895.
[26] K. Punia, M. Bucaro, A. Mancuso, C. Cuttitta, A. Marsillo, A. Bykov, W. L'Amoreaux, K. S. Raja, *Langmuir.* **2016**, *32*, 8748–8758.
[27] W. R. Moore, S. E. Graves, G. I. Bain, *ANZ J. Surg.* **2001**, *71*, 354–361.
[28] H. Sohn, J. Oh, *Biomater. Res.* **2019**, *23*, 9.
[29] I. Drosse, E. Volkmer, R. Capanna, P. De Biase, W. Mutschler, M. Schieker, *Injury.* **2008**, *39*, S9–S20.
[30] S. V. Dorozhkin, M. Epple, *Angew. Chem. Int. Ed.* **2002**, *41*, 3130–3146; *Angew. Chem.* **2002**, *114*, 3260–3277.
[31] L. M. Grover, A. J. Wright, U. Gbureck, A. Bolarinwa, J. Song, Y. Liu, D. F. Farrar, G. Howling, J. Rose, J. E. Barralet, *Biomaterials.* **2013**, *34*, 6631–6637.
[32] L. Mayen, N. D. Jensen, D. Laurencin, O. Marsan, C. Bonhomme, C. Gervais, M. E. Smith, C. Coelho, G. Laurent, J. Trebosc, *et al., Acta Biomater.* **2020**, *103*, 333–345.
[33] M. Pujari-Palmer, S. Pujari-Palmer, X. Lu, T. Lind, H. Melhus, T. Engstrand, M. Karlsson-Ott, H. Engqvist, *PLoS One.* **2016**, *11*, e0163530.
[34] L. Zhu, D. Luo, Y. Liu, *Int. J. Oral Sci.* **2020**, *12*, 6.
[35] T. Tian, J. Liao, T. Zhou, S. Lin, T. Zhang, S. R. Shi, X. Cai, Y. Lin, *ACS Appl. Mater. Interfaces.* **2017**, *9*, 30437–30447.
[36] G. Angelis, D. N. Zayed, A. Karioti, D. Lazari, E. Kanata, T. Sklaviadis, G. Pampalakis, *Chem. A Eur. J.* **2019**, *25*, 12916–12919.
[37] B. C. Batista, P. Cruz, O. Steinbock, *ChemPhysChem.* **2015**, *16*, 2299–2303.
[38] P. Kumar, D. Horváth, Á. Tóth, *Soft Matter.* **2020**, *16*, 8325–8329.
[39] D. Kaigler, Z. Wang, K. Horger, D. J. Mooney, P. H. Krebsbach, *J. Bone Miner. Res.* **2006**, *21*, 735–744.
[40] K. J. Leach, D. Kaigler, Z. Wang, P. H. Krebsbach, D. J. Mooney, *Biomaterials.* **2006**, *27*, 3249–3255.
[41] D. H. R. Kempen, L. Lu, A. Heijink, T. E. Hefferan, L. B. Creemers, A. Maran, M. J. Yaszemski, W. J. A. Dhert, *Biomaterials.* **2009**, *30*, 2816–2825.
[42] A. Hernández, E. Sánchez, I. Soriano, R. Reyes, A. Delgado, C. Évora, *Acta Biomater.* **2012**, *8*, 781–791.
[43] G. E. Friedlaender, C. R. Perry, J. D. Cole, S. D. Cook, G. Cierny, G. F. Muschler, G. A. Zych, J. H. Calhoun, A. J. LaForte, S. Yin, *J. Bone Jt. Surg.* **2001**, 83-A, S151–S158.
[44] E. Alsubhe, A. D. Anastasiou, M. Mehrabi, E. M. Raif, A. Hassanpour, P. Giannoudis, A. Jha, *Mater. Sci. Eng. C.* **2020**, *115*, 111053.

Manuscript received: December 21, 2020
Accepted manuscript online: January 22, 2021
Version of record online: ■■, ■■■

ARTICLES

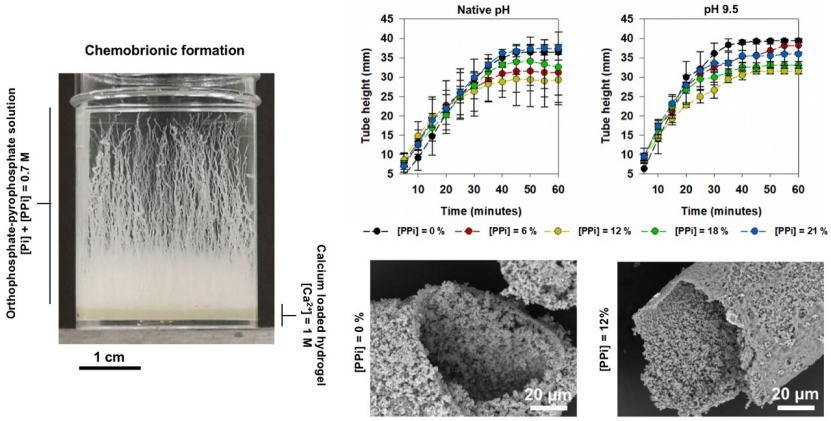

Dr. E. A. B. Hughes, O. Jones-Salkey, P. Forey, M. Chipara, Prof. L. M. Grover**

Special Collection

Chemical gardens: Hierarchical tubular microstructures composed of calcium orthophosphate-pyrophosphate are grown using a chemobrionic hydrogel-solution system. These biologically relevant chemical garden systems may be of interest to the field of regenerative medicine, particularly in the development of biologically responsive biomaterials for hard tissue regeneration.